Identification of carbon species on iron-based catalysts during Fischer-Tropsch synthesis

Diego Peña[a], Andrea Cognigni[a], Thomas Neumayer[a], Wouter van Beek[b], Debra S. Jones[c], Melesio Quijada[d], Magnus Rønning[a.]*

[a] *Department of Chemical Engineering, Norwegian University of Science and Technology, 7491 Trondheim, Norway.*
[b] *The Swiss-Norwegian Beamlines at ESRF, BP 220, F-38043 Grenoble, France.*
[c] *Johnson Matthey Technology Centre, Blount's Court, Sonning Common, Reading RG4 9NH UK.*
[d] *Laboratoire GEOSYSTEMES, UMR 8217, Université Lille 1, Bât. SN5, Cité scientifique, 59655 Villeneuve d'Ascq, France.*

Abstract

This paper focuses on the use of *in situ* and *ex situ* characterisation techniques to provide evidences of carbon species on a commercial iron-based Fischer-Tropsch synthesis catalyst as well as other indices of potential deactivation mechanisms. *In situ* XANES measurements demonstrate that re-oxidation or transformation of the active iron phase, i.e. the Hägg carbide phase, was not a significant deactivation mechanism at the studied conditions. Sintering of Hägg carbide nanoparticles is significant with increasing temperatures and time on stream. The sintering mechanism is proposed to be a hydrothermally-assisted process. *In situ* DRIFTS indicates the presence of different carbon species on the catalyst surface such as aliphatic hydrocarbons from wax products and oxygenate compounds such as alcohols, aldehydes/ketones and carboxylate species. Carboxylate species are resistant towards hydrogenation at 280°C. The presence of different carbon species on the surface after wax product extraction is evident from TPH-MS measurements. GC–MS analysis shows that the strongly adsorbed carbon species remaining on the catalyst surface from wax products are mainly α-olefins and branched carboxylic species. The interaction of oxygenate compounds, especially carboxylate species with iron oxide, may form stable complexes limiting further iron catalyst carburization. STEM-EDX analysis shows that carbon is preferentially located on iron particles.

Keywords: Fischer-Tropsch synthesis; *in situ* characterization; iron catalyst; surface species

1. Introduction

The presence of deactivation mechanisms in Fischer-Tropsch synthesis (FTS) catalysts have been investigated since the first work on these catalysts in the early 1920s [1,2]. However there is still much debate and controversy concerning the main reasons for the eventual loss of catalytic activity [3]. Despite this, there is a consensus regarding the stability and resistance to deactivation of the most common FTS catalysts i.e. cobalt-based and iron-based catalysts. The productivity of cobalt-based catalysts at high conversion is currently higher than that of iron-based catalysts. On the other hand, iron-based catalysts are more prone to deactivation as they are further susceptible to carbon deposition, re-oxidation/ transformation of active phases, sintering and catalyst attrition [1,3,4]. Iron-based catalysts are seen as an attractive option for the Biomass-To-Liquid (BTL) process, because of their capacity to manage different syngas feed ratios (H_2/CO= 0.5-2.5) including syngas rich in CO_2, since they also catalyse the water-gas-shift (WGS) reaction [1]. In addition, they have the ability to work at higher temperatures with low methane production, higher sulphur tolerance (<0.2 ppm) and less expensive catalyst production, which impacts on the cost of the entire process [1,2,4] . Operating the FTS unit with a CO_2 rich feed without purification could result in a simpler, lower cost process [5,6]. Hence, the improvement of current iron-based catalysts is desired. Fundamental research on commercial and model catalysts is crucial to understand deactivation mechanisms during FTS. It may open up possibilities to propose deactivation pathways, decoding their effect on surface chemistry of the catalysts and thus catalytic performance. Based on such research, it may be possible to

propose better catalyst formulations, preparation routes and activation procedures as well as deactivation-modelling studies. Due to the complexity of the FTS, the study of deactivation mechanisms requires the use of advanced characterisation techniques. For example; studying of re-oxidation of active phases, which are very sensitive to changes by oxygen from air[3], must be done under *operando/in situ* conditions. For that purpose, *in situ* synchrotron techniques such as X-ray absorption fine structure spectroscopy (XAFS) combined with powder X-ray diffraction (XRD) [7–10] have been shown to be very useful to study active phases in their working environment. XAFS may be divided in two spectral regions; the X-ray absorption near edge structure (XANES) and extended X-ray absorption fine structure (EXAFS) provide detailed information about the oxidation state and coordination of the absorber atoms [11]. *In situ* XAFS can be employed as a bulk characterisation technique to identify and quantify the different iron oxide and carbide species present during FTS at relevant working conditions [11–17]. *In situ* XRD can bring information related to the crystallinity and sintering [18]. Several carbide species such as ε-Fe_2C, ε′-$Fe_{2.2}C$, Fe_7C_3, χ-Fe_5C_2, and θ-Fe_3C have been detected [3]. χ-Fe_5C_2 and θ-Fe_3C [11,12,19–22] are normally the most stable and common species during FTS. High CO conversion rate and hydrocarbon productivity have been associated with χ-Fe_5C_2 (Hägg carbide) while catalyst deactivation due to carbon depostion can be associated with θ-Fe_3C (cementite) [14,23,24] . Iron carbide clusters are usually pyrophoric and are therefore readily transformed into iron oxides when exposed to air [3]. Synchrotron X-ray *in situ* methods in characterising bulk and supported catalysts are excellent tools for studying active site formation/evolution in FTS catalysts [25]. *In situ* XRD is a suitable characterisation technique to measure the degree of sintering since pyrophoric iron carbides [3,12] are preserved without external influence of oxygen from air. Catalyst attrition arising from degradation of catalyst particles into finer particles is mainly observed in slurry and fluidised-bed reactors [26–33], but less pronounced in fixed-bed reactors. Carbon deposition as a potential deactivation mechanism is difficult to investigate due to the accumulation of detrimental carbon species on the catalyst surface being masked by the presence of hydrocarbon wax products. Although it is hard to differentiate between them, polymeric carbon has been identified as the most deleterious of carbon species [34]. It is believed that this carbon is formed from the polymerisation of CH_x and has an alkyl group structure making it less reactive. The resilient carbon species on spent cobalt-based catalysts have been characterised by many ex situ techniques; they are mainly composed of aliphatic hydrocarbons like α-olefins and oxygenates such as carboxylic acids, aldehydes, ketones and alcohols. Oxygenates showed special affinity to the acid sites of the support [35,36]. Moreover, it has been reported that carboxylic acids can cause atomic carbon formation on cobalt-based catalysts during FTS as a result of strongly adsorbed carboxylate species on the support [37]. In addition, once adsorbed, they can accumulate on catalyst surface and generate steric hindrance [36], probably leading to a decay in catalytic activity. *In situ* diffuse reflectance infrared Fourier transform spectroscopy (DRIFTS) has recently been used to determine the nature/reactivity of surface carbon species under FTS conditions on cobalt-alumina catalysts, suggesting the presence of aliphatic species related to wax products and oxygenate species associated with formate and carboxylate [38,39]. Results also indicate strong interaction of oxygenate compounds, especially carboxylate species, with oxidic sites and the catalyst support. Beyond the previously mentioned, very little information can be found in the open literature about the use of *in situ* and ex situ characterisation techniques to investigate deactivation mechanisms on iron-based FTS catalysts. Hence, this work makes use of several *in situ* and ex situ characterisation techniques to provide insight into potential deactivation mechanisms on a commercial iron-based catalyst under relevant operating conditions.

2. Experimental

2.1. Commercial catalyst and carbide references

The catalyst used in this study was a Fe-based co-precipitated catalyst provided by Johnson Matthey. The catalyst is composed of Fe_2O_3, SiO_2, CuO, K_2O and Na_2O. Before *in situ* characterisation, the catalyst was crushed and sieved to particles between 38-106 μm diameters. The spent catalyst for ex situ characterisation was recovered after the sample was pre-treated under pure CO for 7 hours at 210°C and then exposed to FTS at 280°C, H_2/CO=2, 20 bars and GHSV ~ 600 $LKg_{cata}^{-1}h^{-1}$ in a fixed bed reactor, and maintained for 120 hours. For carbon

characterisation, the hydrocarbon wax-product was extracted from the spent catalyst via Soxhlet extraction, using similar methodology to what has been reported elsewhere [35,40]. For the identification of carbide species present in the spent catalysts, two carbide references were synthesised using the procedure reported by de Smit et al. [12]:

- Hägg carbide (χ-Fe_5C_2) reference: A commercial sample of Fe_2O_3 (Sigma-Aldrich, 99% < 5 microns) was reduced in pure CO at 350°C for 4 h (ramping rate of 4°Cmin^{-1}) at atmospheric pressure.

- Cementite carbide (θ-Fe_3C) reference: A commercial sample of Fe_2O_3 (Sigma-Aldrich, 99% < 5 microns) was reduced in pure CO at 450°C for 4 h (ramping rate of 4°Cmin^{-1}) at atmospheric pressure.

2.2. In situ XANES /XRD/MS combined set-up

The *in situ XANES* /XRD measurements were collected at the Swiss-Norwegian beam lines (BM01B) at the European Synchrotron Radiation Facility (ESRF) in Grenoble, France. The crystallinity and composition of the different iron phases were monitored by *in situ* XRD and XAFS, respectively. Around 6 mg of the catalyst precursor was placed inside a capillary reactor (1.0 mm outer diameter) giving a bed length of about 10 mm. This type of capillary reactor has shown quasi plug flow reactor performance especially designed for X-ray applications [41]. The reactor was mounted in a stainless steel bracket and sealed with high temperature epoxy glue. The sample was pre-treated ex situ with pure CO at 210°C for 7 hours at ambient pressure and kept sealed in He atmosphere. The measurements were carried out at 230°C, 250°C and 280°C, 18 bar, gas hourly space velocity (GHSV) ~15000 LKg$cata^{-1}h^{-1}$, syngas 64% vol. H_2, 32% vol. CO and Ar 4% vol. Firstly, He was introduced to achieve the working pressure (18 bar) with the pressurization taking approximately 1 hour. After ensuring no leaks, the temperature was increased from room temperature to 230°C using a ramp rate of 5°Cmin^{-1} under syngas (~6 h for each temperature step). XRD and XANES data were alternately collected together with on-line MS data. A cycle of measurements took around 1 hour, i.e. one X-ray diffractogram (25 min) and six XANES spectra (5 min). The ion chambers were optimised for iron K-edge energy (7112 eV) detection. Qualitative and quantitative analysis were carried out on the XANES part of the XAS spectra. The experimental set-up and the protocol of *in situ* measurements are described in detail elsewhere [42].

2.3. In situ DRIFTS measurements

DRIFTS experiments were performed at ambient pressure with a Praying Mantis™ high-temperature DRIFTS reaction cell from Harrick Scientific Corporation with ZnSe windows. A detailed description of the reaction cell and the experimental set-up can be found elsewhere [42]. The sample was diluted with KBr (3:1) in order to obtain a good signal to noise ratio. The contribution from the gas-phase was subtracted using the syngas spectrum collected over pure KBr at the different reaction temperatures. Initially, the fresh catalyst was heated to 230°C under He atmosphere, then the syngas was introduced (1 mLm^{-1} H_2, 0.5 mLm^{-1} CO, H_2:CO 2:1) while collecting spectra for approximately 3 h at each temperature. The system was operated at atmospheric pressure and the GHSV was about 1200 LK$g_{cata}^{-1}h^{-1}$. The analysis was performed mainly in the alkane and oxygenate regions to detect potential accumulation of such species on the catalyst surface with time on stream.

2.4. Ex situ characterization techniques

The XRD patterns of the fresh and spent samples were obtained by using a Bruker D8 Advance DaVinci instrument with a Cu anode (λ=1.54 Å). The samples were run for 120 min in the range 2θ = 10-75°. The phase identification and the crystallite size of the catalysts were acquired in the evaluation software Diffrac.eva. Differential scanning calorimetry - thermal gravimetric analysis (DSC-TGA) was carried out using a Netzsch Jupiter 449 instrument. The analyses were performed in pure argon at temperatures ranging from room temperature to 900°C with the aim of determining the weight loss related to desorption and decomposition of carbon species. The helium flow rate was 100 mLmin^{-1}, 20 mg sample loading and a heating rate of 10°Cmin^{-1} was

used. The mass loss of the catalyst was recorded and the component mass of the residues was measured by a QMS 403C Aëolos® quadrupole mass spectrometer (MS). In order to differentiate the reactivity of each carbon species towards hydrogen, temperature programmed hydrogenation (TPH) was carried out using an Altamira AMI-300 instrument coupled with a gas analyzer system/mass spectrometer (MS) Pfeiffer Vacuum QMG 220. About 50 mg of catalyst was used for the TPH-MS analysis and the temperature was ramped 4°Cmin^{-1} under pure H_2 at 50 mL.min^{-1} from room temperature to 700°C at atmospheric pressure. The evolution of methane (m/z = 15, instead of 16 to avoid interference from ionised oxygen coming from water vapour) [21] and C_xH_y (m/z = 28 fragment, which corresponds to the C_2 fragment from hydrocarbons) were simultaneously monitored; using similar approach previously reported [35]. Transmission electron microscopy (TEM) experiments were performed with a JEOL 2010F instrument equipped with a field emission gun, operating at 200 kV accelerating voltage. The samples were prepared by dispersion of the crushed catalysts powder on a carbon supported Au mesh grid. Element mapping of the samples was performed in scanning transmission electron microscopy (STEM) mode coupled with energy-dispersive X-ray spectroscopy (EDX) detection. Carbon, silicon and iron maps in the catalyst were obtained by acquiring series of spectra when scanning the EDX probe that collect the X ray signal coming from specific atoms excitations due to the electron beam at the surface of a region of interest. At each pixel of the scan (0.5 nm x 0.5 nm) full EDX spectrum is acquired. The whole set of EDX spectra is then processed to obtain the chemical atom map. Organic compounds were extracted from ~ 100 mg of the catalysts mixed with 5 mL of dichloromethane by ultrasonic agitation at 20 kHz for 15 min (HF power: 100 W max; Bandelin Sonopuls). After centrifugation at 5000 rpm for 2 min, the supernatant was collected. The resulting total extract was rotary-evaporated to dryness at a temperature not exceeding 40°C. The extracts were separated over an activated silica column using cyclohexane (Cy) to recover the aliphatic fraction, a mixture of Cy/ dichloromethane (DCM) 2:1 (v/v) to recover the aromatic fraction, and a mixture of DCM/MeOH 2:1 (v/v) to recover the most polar fraction. 1 µL of extract was injected into a gas chromatograph (Perkin Elmer 680) coupled with a mass spectrometer (Perkin Elmer 600). Gas chromatographic conditions were as follows; inlet heated at 250°C, DB5-MS-UI column initially at 40°C for 1 min and heated to 320°C at 10°C.min^{-1} and maintained 10 min at 320°C, helium column flow of 1 mL.min^{-1}, split ratio of 10. Mass spectrometer conditions were as follows; mass scan 45–500, scan time 0.2 s, interdelay scan 0.1 s, ionisation energy 70 eV. The identification of compounds was based on the comparison with the NIST mass spectra database and/or on the comparison of retention times of standards.

3. Results and discussion

3.1. Iron phase identification (potential re-oxidation)

The identification of iron phases during FTS was performed by *in situ* XANES. The evolution of those phases was monitored by a linear combination fitting (LCF) of the XANES part of the spectra with selected iron references [11,12,14] such as wüstite (FeO), hematite (Fe_2O_3), magnetite (Fe_3O_4), cementite (Fe_3C), metallic iron (Fe^0) and Hägg carbide (Fe_5C_2). The Athena software package [15] was employed for the analysis. Fig. 1(a) displays the XAFS data set evolution during FTS at the different temperatures and Fig. 1(b) presents the XANES LCF results showing the evolution of fractions of the different iron phases identified.

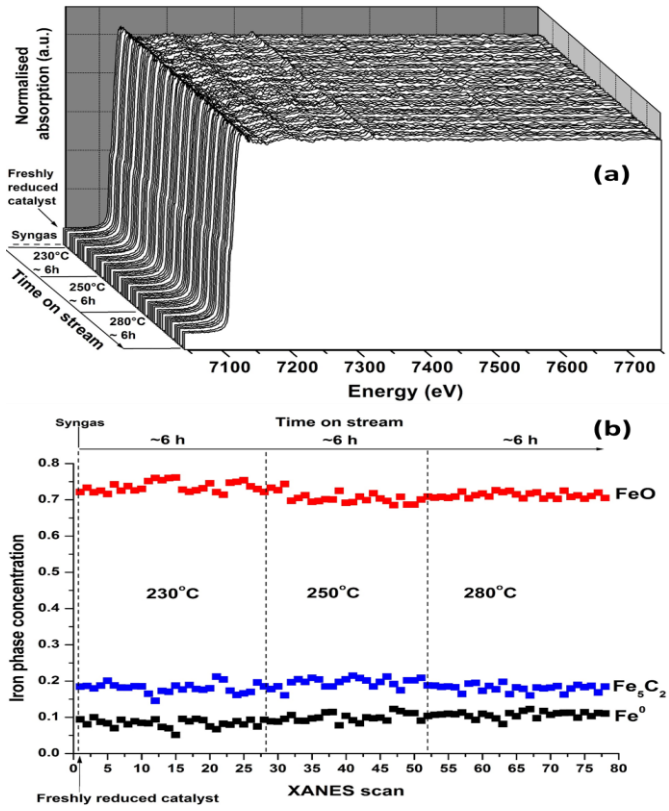

Fig.1. (a) *In situ* XAFS data set evolution and (b) the XANES LCF results showing the fractions of Fe species.

The XAFS data evolution did not show any abrupt changes in absorption intensity and energy shifts before and after syngas feeding even at higher temperatures. Both, pre-edge and the white line showed features characteristic of metallic iron and iron carbide phases [11,12,43,44]. XANES analysis of the freshly reduced catalyst (CO pre-treated at 210°C ~ 7 h) showed FeO, Fe_5C_2 and Fe^0 as the major iron phases. The metallic iron phase and carbide fractions were very stable during the experiment, even at higher temperatures and extended time on stream. The metallic iron phase is most likely γ-Fe since it has a more stable structure resistant to carbon accumulation compared to α- Fe [11]. Transformation of Fe_5C_2 to less active carbide such as Fe_3C or even re-oxidation of metallic/iron carbide phases into Fe_3O_4 was not observed. It is widely known that FeO is stable in the presence of SiO_2 [45] due to a strong FeO-SiO_2 interaction [46] which can suppress further reduction of FeO into Hägg carbide. Table 1 summarizes the fractions of FeO, metallic iron and Hägg carbide taken from the freshly reduced catalyst exposed to FTS conditions and *in situ* measured at the end of each isothermal step.

Table 1. Summary of iron phase concentration from XANES during FTS at 18 bar, H_2/CO =2, 230-250-280°C.

Temp. (°C)	Freshly reduced (CO pre-treated)	230	250	280
(%) FeO	73 ± 3	71 ± 4	69 ± 4	70 ± 3
(%) Fe (0)	9 ± 2	9 ± 3	11 ± 3	11 ± 2
(%) Fe_5C_2	18 ± 2	20 ± 2	20 ± 3	19 ± 2

The concentrations of the different iron phases were almost constant even at higher temperatures, meaning that the iron phases in the freshly reduced catalyst were stable during FTS. It is important to emphasize that, under the applied conditions, there is probably a maximum degree of Fe^0 and Fe_5C_2 formation [47] where re-oxidation and transformation to less active carbide was limited. The FeO phase stability is probably due to the strong FeO-SiO_2 interaction. The iron phase concentrations are also governed by the thermodynamic equilibrium of the system, since they are influenced by the H_2 and CO partial pressures and the reaction temperature [48].

There is a lot of controversy in the literature about the nature and re-oxidation of iron active phases during FTS [2,3,11,12,14,19–21,24,49–54]. It is believed that both metallic Fe and Fe carbides are considered active phases that can dissociate and hydrogenate CO [55]. Under FTS conditions, carbide phases readily form due to the proposed similarity between the activation energy barriers of carbon diffusion into the metallic Fe body to form carbide (43.9-69.0 kJ mol^{-1}) and hydrogenation and polymerization at the catalyst surface (89.1±3.8 kJ mol^{-1}) [3,12]. Therefore, carbide formation must occur before the catalyst surface can retain sufficient carbon to become active [55]. In the present case, metallic iron and Hägg carbide phases were both detected. It is known that both species can be oxidised by produced water, but in iron systems H_2O is mainly consumed by the WGS reaction although CO_2 formed as by-product from this reaction also has the capacity to re-oxidise carbide phases [19,52]. It has been reported [12,19,20] that χ-Fe_5C_2 carbide can be transformed with increasing concentrations of H_2O and CO_2 into θ-Fe_3C and further to Fe_3O_4 while metallic iron is oxidised directly into Fe_3O_4. Iron phase re-oxidation by CO_2 or H_2O was not observed in the present study. Based on our results, it is possible to discard re-oxidation as a potential deactivation mechanism at these conditions. It has also been reported that the build-up of H_2O pressure in the FTS catalyst pores is often regarded as the main reason for catalyst oxidation, leading to the formation of a core-shell oxide-carbide structure [12], but this is not present in our catalyst. Further characterisation studies were carried out to determine the presence of other potential deactivation mechanism such as sintering and/or carbon deposition.

3.2 Sintering of iron nanoparticles

The *in situ* XRD patterns of the freshly reduced catalyst (CO pre-treated at 210°C ~ 7 h) showing crystalline iron phases during FTS conditions are displayed in Fig 2.

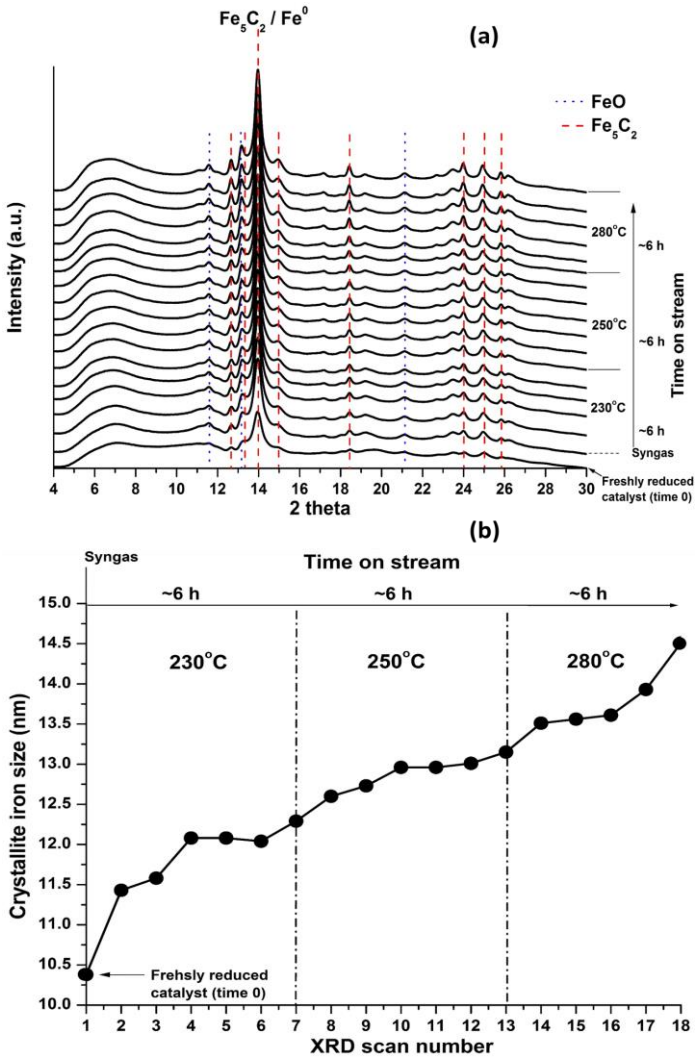

Fig.2. (a) *In situ* XRD crystalline phase evolution and (b) average Fe_5C_2 crystallite size growth as a function of temperature

Diffraction lines were detected at 2θ= 12.8°, 13.9°, 18.2°, 24° 25° and 25.8° characteristic of the presence of Hägg carbide (PDF04-013-0092) [12] crystallites of around 10 nm as well as other contributions associated with FeO, which confirm that the catalyst is mainly composed of Fe_5C_2 and FeO iron-phases. There is no evidence of crystalline iron phase transformations although an increase in intensity with time on stream of the main diffraction signal of Fe_5C_2 was observed, indicating particle sintering [56]. This diffraction line at 2θ ~ 13.9 is also close to the main diffraction reported for metallic iron at 2θ ~ 14.2 (PDF04-014-0360) [12]. The presence of the same phases as previously detected by *in situ* XANES can be also observed by XRD. Janbroers et al. [57] reported a similar diffraction pattern for an iron-based catalyst activated under pure CO at 270°C, suggesting the presence of both iron-phases. The estimation of the average crystallite size evolution was calculated from the main diffraction line at 2θ ~ 13.9 using the Scherrer equation [58]. As can be observed from Fig. 2 (b), the iron carbide/$Fe^{(0)}$ nanoparticles grow in size, starting from around 10.5 nm on the freshly reduced catalyst and ending at around 15 nm according to the last measurement at 280°C under FTS conditions. This is consistent with previous findings that examined the sintering of carbide nanoparticles by *in situ* TEM [57]. Based on the Gibbs free energy some FTS products such as methane and light products such as methylene are most favoured with increasing temperature [36]. Water is also favoured according to the carbon monoxide hydrogenation reaction stoichiometry using syngas ratio of 2:1: $CO + 2H_2 \rightarrow -CH_2- + H_2O$ where one methylene monomer and one molecule of water are formed. We therefore suggest a hydrothermal sintering process [49] assisted by the produced water and high temperature [4] simultaneously with the water-gas shift reaction taking place. A schematic representation of these proposed simultaneous processes is shown in Fig. 3.

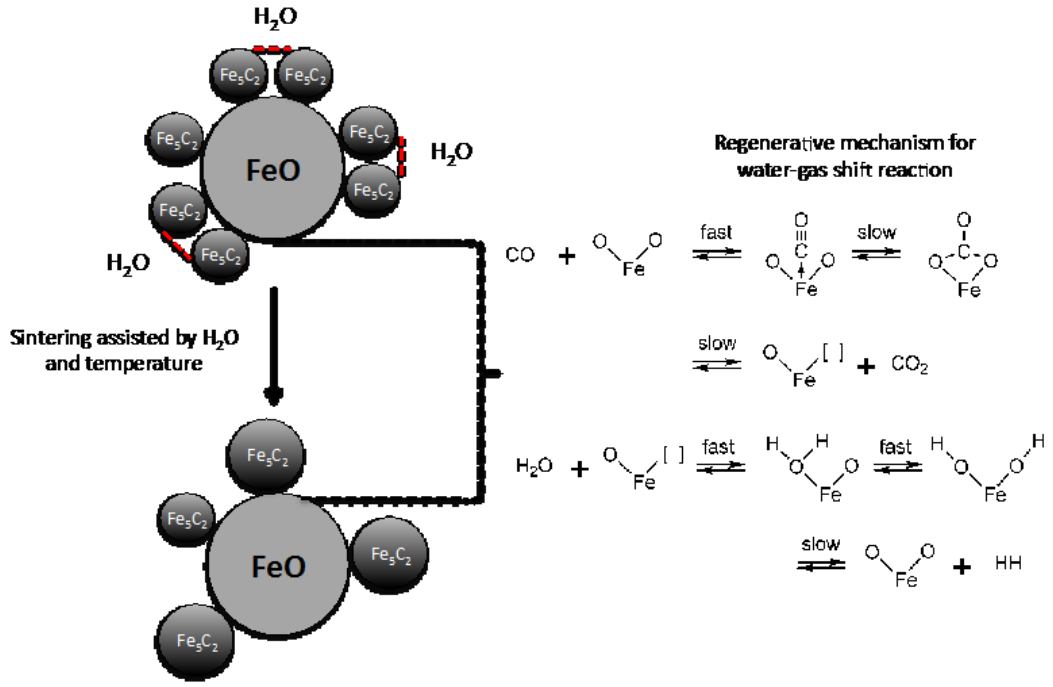

Fig. 3. Simultaneous hydrothermal sintering and water-gas shift reaction (adapted from reference [3] with permission from the Royal Society of Chemistry).

Once the syngas is introduced, the water produced during FTS might activate the sintering of carbide nanoparticles on the catalyst surface. In addition, an increase in temperature can usually raise the rate of sintering (Fig. 2 (b)). Most likely, water molecules first activate the sintering process and then participate in the water gas-shift reaction following the regenerative mechanism postulated by de Smit et al. [3] in the presence of FeO on the catalyst surface. The active site in this mechanism is the anion–cation pair site (FeO sites on our catalyst) where CO coordinates to the iron cations and reacts with the associated surface oxygen atoms to form a bidentate carbonate. Then CO_2 is liberated from the surface, leaving behind a surface oxygen vacancy. On this site, water (after having assisted the sintering of iron carbide) can be adsorbed, filling the oxygen vacancy and subsequently desorbing H_2. In our working iron-based catalyst, the presence of two types of active sites is suggested; first Fe_5C_2 sites responsible for FTS activity and second FeO sites that catalyse the WGS reaction (Fig. 3).

For iron catalysts it is generally accepted that the formation of hydrocarbons can be explained by the surface carbide mechanism [3,5,6], although it cannot explain the formation of oxygenates. CO insertion into the growing chain has been postulated to justify the formation of oxygenates [59]. Moreover, iron catalysts show higher selectivity toward oxygenated products than cobalt catalysts [2] due to their tendency to adsorb CO molecularly with slower dissociation rates than cobalt catalysts and also due to a stronger oxophilicity [60], leading to incorporation of more oxygen in the products. According to Pérez-Alonso et al. [61], besides catalysing the WGS reaction, the FeO phase could also increase the selectivity towards oxygenated products. Therefore, the presence of some oxygenate species coming from intermediates and products is expected on iron catalyst surfaces at FTS conditions.

3.3 Carbon deposition

There are three principal challenges related to the characterisation of carbon during FTS: (i) identification of the nature and reactivity of different carbonaceous species including products, intermediates and surface species; (ii) differentiating between the resilient carbon species and other species and finally; (iii) defining the location of these resilient carbon species. In the next section, these challenges were approached by focusing on oxygenate compounds and their probably role in decreasing catalytic performance.

3.3.1. In situ characterisation

In situ diffuse reflectance infrared Fourier transforms spectroscopy (DRIFTS) measurements have proved to be an efficient tool for decoding the nature and reactivity of surface species during FTS for cobalt catalysts, but not yet widely employed for iron-based catalysts. Fig. 4 displays the *in situ* DRIFTS measurements carried out on our commercial iron-based catalyst during activation under pure CO and during FTS conditions at atmospheric pressure.

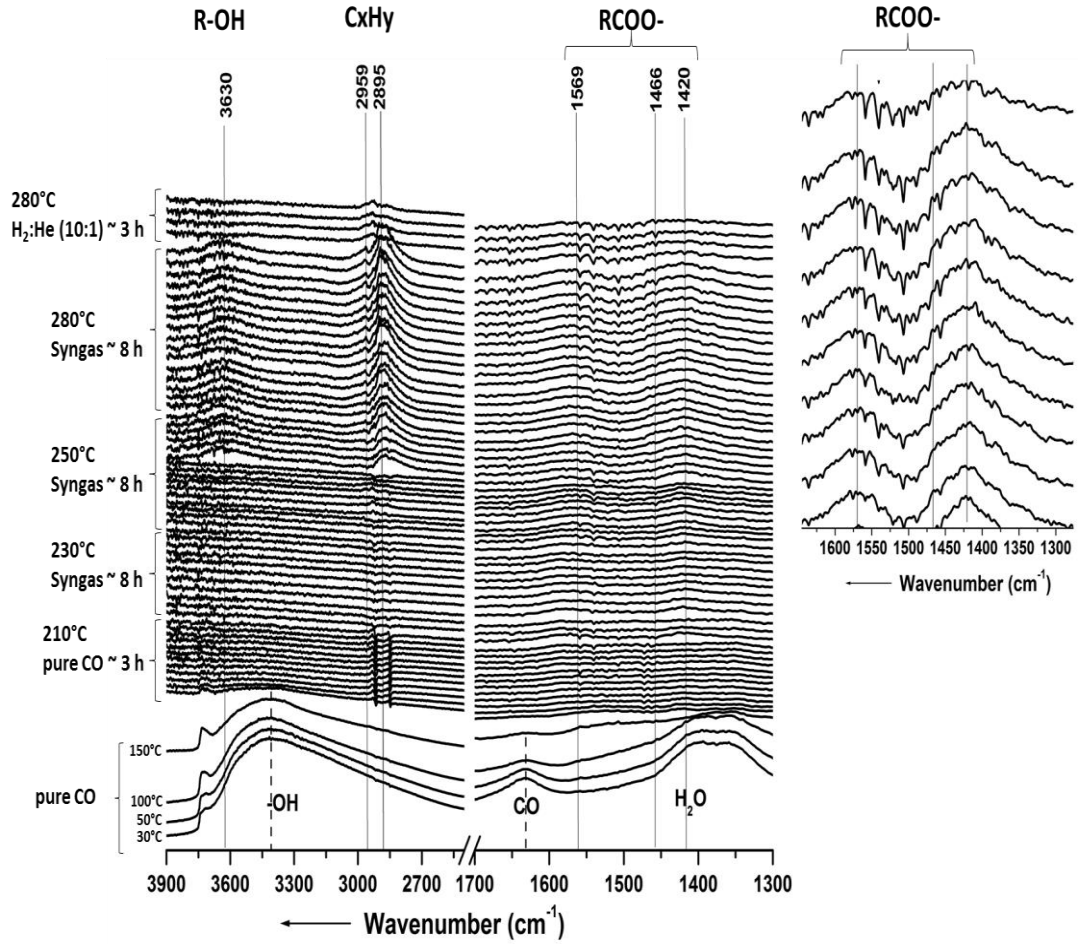

Fig.4. *In situ* DRIFTS spectra collected during the activation step under pure CO, FTS using syngas H_2:CO (2:1) at three different temperatures and under H_2 diluted with He (10:1).

When heating the sample during pre-treatment in pure CO, bands related to adsorbed molecular water at around 1400-1450 cm^{-1}, carbonyl adsorption at around 1630 cm^{-1} [35] and hydrogen bonding from water and hydroxyl groups in the region between 3800-2700 cm^{-1} [39] were observed. At 210°C almost total desorption of these groups was achieved. After maintaining this temperature for 3 h, the measurements showed a virtually flat signal. After that, the sample was heated to 230°C and then syngas was introduced. At this temperature, only two wide bands appeared around 1569 cm^{-1} and 1420 cm^{-1}. However, after some hours at 250°C other bands at 3630, 2959 and 2895 cm^{-1} also appeared. These additional bands were further developed at 280°C with increasing time on stream. The band at 3630 cm^{-1} can be associated with the stretching vibration of "free" O-H groups most likely coming from alcohols [62] over the catalyst surface while the bands at 2959 and 2895 cm^{-1} can be related to the stretching vibrations of methylene (-CH -) groups [63] originating from alkane chain formation leading to wax products. At lower wavenumbers, broad bands increased in intensity with time on stream at 1569, 1466, 1420 cm^{-1} which can be assigned to carboxylate species [64,65]. An expansion of these carboxylate bands is shown in the right top corner of Fig. 4. D. Lorito et al. [38] suggested that formate species could be potential intermediates in the formation of methanol. In our case, no bands related to formate species were detected, which may indicate that they are immediately

hydrogenated to alcohols as suggested by the continuous band related to O-H groups at 3630 cm^{-1}. In addition, no bands related to aromatic compounds on the catalyst surface were detected. Ning et al. [66] reported that graphite-like carbonaceous compounds were not detected by laser Raman spectroscopy (LRS) in spent iron-based FTS catalysts under comparable operating conditions. Similarly, Das et al. [67] have reported the olefinic rather than graphitic nature of carbon deposited on the surface of spent iron catalysts after FTS. More severe reaction conditions in terms of higher temperatures and higher pressure or lower syngas ratio are needed to form aromatics species [35, 68].

The bands related to alcohols disappeared and aliphatic hydrocarbons almost completely vanished when syngas was changed to a stream rich in H_2 at 280°C, while the bands related to carboxylate species were still present but less intense. The presence of strongly adsorbed carboxylate species has been previously detected for cobalt-based FTS catalysts. Paredes-Nunez et al. [39] reported that the IR band related to carboxylate species adsorbed on alumina can remain unaffected in the presence of hydrogen. Peña et al. [35] have also observed the presence of resistant-branched carboxylic acids strongly adsorbed on the alumina surface of spent Co-based FTS catalysts. Kistamurthy et al. [37] reported that carboxylic acids can cause elemental carbon formation on Co-based alumina catalysts during FTS as a result of strongly adsorbed carboxylate species on alumina, which probably generate steric hindrance once adsorbed on the catalyst surface [36]. de Smit et al. [69] observed by *in situ* XPS the formation of carbonate species during syngas treatment over an iron-based catalyst at atmospheric pressure during FTS. They also reported that the carbonate species could hinder carbide formation and that they slowly desorb at higher temperatures up to about 450°C [70]. Moreover, it has been reported that the iron cations Fe^{2+} and Fe^{3+} can form separate complexes with carboxylate ligand groups [71]. Based on the literature and our results, the carboxylate species and probably also carbonate detected by *in situ* DRIFTS could form complexes with Fe^{2+} from FeO (the most abundant iron oxide species detected by *in situ* XAFS). These complexes could suppress further carburization of the iron catalyst, as suggested also in our previous work [42].

3.3.2. Ex situ characterisation

Ex situ characterisation of carbon species was carried out on a spent catalyst subjected to FTS for around 70 h, where an amount of carbon deposit containing different species had accumulated [34]. The carbon species from the spent catalyst surface were extracted using an organic solvent mixture (CH_2Cl_2:CH_3OH 2:1) using a similar analysis protocol as explained elsewhere [35,36]. Fig. 5 displays a typical total ion current (TIC) and mass fragmentogram of the most abundant species detected.

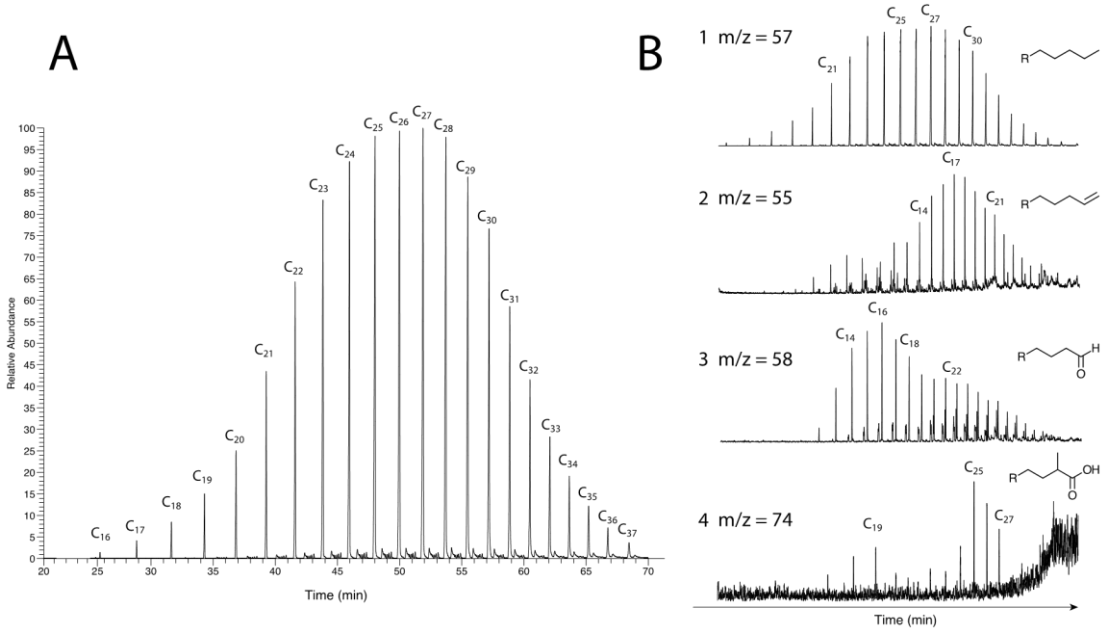

Fig. 5. Chromatogram of the organic-extract from spent catalyst CO activated-longer test: (a) Total ion current (TIC) and (b) ion mass fragmentogram of the identified species. Numbers above the peaks represent carbon number.

High relative abundance of a set of linear aliphatic hydrocarbons corresponding to *n*-paraffins was identified as the dominant species on the spent catalyst surface. Apart from the ion fragment m/z = 57 corresponding to *n*-paraffins, other compounds were identified such as α-olefins by the ion mass m/z =55 and oxygenates such as 2-methyl fatty acids and 2-methyl aldehydes/2-ketones from the ion mass m/z =74 and m/z = 58 MacLafferty rearrangement, respectively [35]. Alcohols could not be detected. It is known that alcohols form hydrogen-bonded network R-O-H· · ·O-H-R complexes which make their analysis difficult by GC–MS [72]. Nevertheless, GC-MS results are in good agreement with the *in situ* DRIFTS measurements where aliphatic hydrocarbons and oxygenates were identified on the working catalyst surface.

Once the surface carbon species and their molecular structure were defined, the determination of the resilient carbon species was carried out. *In situ* DRFTS measurements suggested carboxylates as resilient species due to their resistance toward hydrogen. The paraffinic wax product on the spent catalyst surface was removed using the Soxhlet extraction method [36,73]. This extraction was previously used to successfully remove wax products from spent cobalt-based catalyst surfaces [35]. The effectiveness of the Soxhlet extraction was proven by XRD analysis of the spent catalyst before and after wax-extraction as observed in Fig. 6.

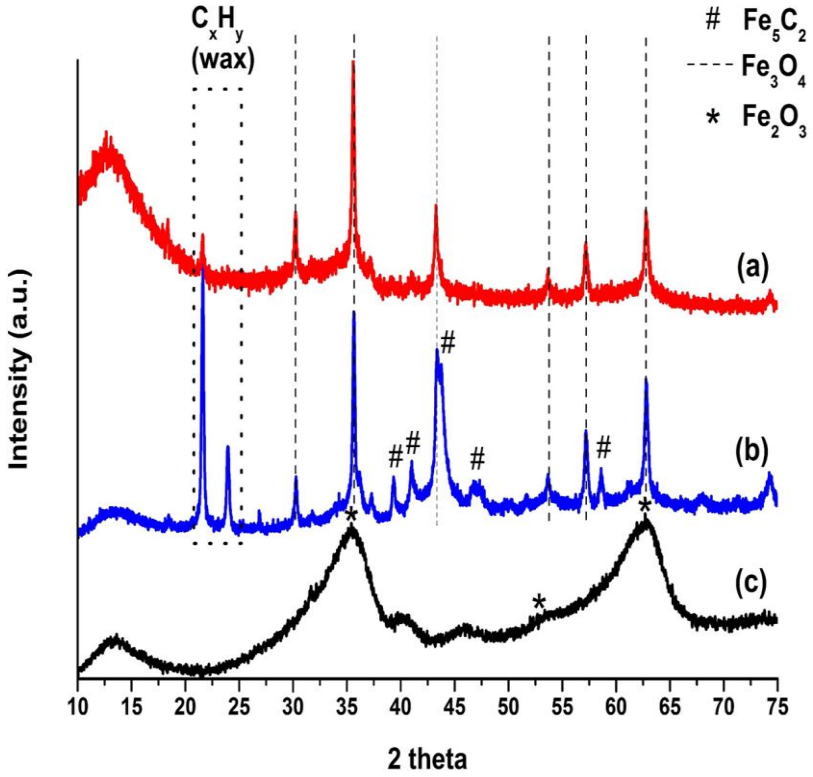

Fig. 6. XRD patterns: (a) spent catalyst after Soxhlet extraction, (b) spent catalyst before Soxhlet extraction and (c) fresh catalyst.

The fresh catalyst displayed hematite as the main iron-oxide crystalline phase. The spent catalyst showed re-oxidation of FeO into Fe_3O_4 after exposure to air, although some diffraction peaks corresponding to Hägg carbide (JCPDS 36-1248) [74] still remain as well as two peak related to wax products [75]. It is possible that waxes are covering Hägg carbide sites and hence protecting them from re-oxidation. Janbroers et al. [57] reported that Hägg carbide could be covered by amorphous carbon preventing its re-oxidation. After Soxhlet extraction, the diffraction peaks corresponding to wax were almost completely removed leaving only magnetite as the major phase. It is also known that iron carbides are readily oxidised in air at room temperature, leading to the formation of mainly Fe_3O_4 [3]. The results suggest that when the catalyst is exposed to air, a fraction is also oxidised to magnetite and after the Soxhlet extraction, the carbide phase is almost totally oxidised.

TGA-DSC analysis was performed under helium in order to determine the weight loss associated with desorption/fragmentation of carbonaceous species remaining on the spent catalyst after wax extraction. Similar analysis has previously been performed on spent cobalt-based FTS catalysts [40]. Fig. 7 displays the TGA-DSC profiles of the fresh catalyst and spent catalyst before and after wax-extraction.

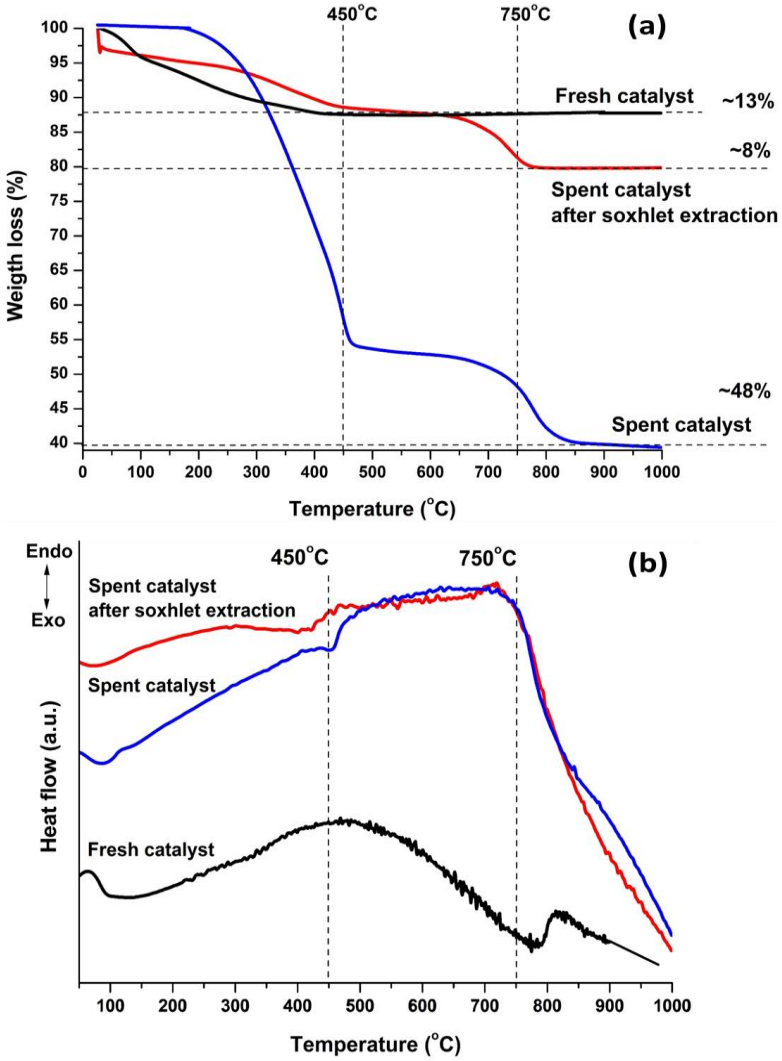

Fig.7. TGA (a) and DSC (b) profiles of the fresh and spent catalyst before and after Soxhlet extraction.

The TGA profile of the fresh catalyst showed a weight-loss of ~ 13% which can be attributed to the removal of chemisorbed water and hydroxyl groups from the catalyst surface [76]. Das et al. [67] stated that for spent iron-based catalysts the weight-loss near 200°C is attributed to volatile wax deposited in the porous structure, while above 580°C the weight-loss corresponds to amorphous carbon combustion. In our case, the observed weight-loss corresponds to fragmentation/desorption of carbon species since helium was used for the analysis instead of air. Based on this statement, for the spent catalyst the TGA-DCS profile displayed two weight-losses one close to 450 °C and the second at around 750°C corresponding to a total weight-loss of about 48%. The first could be attributed to the fragmentation/desorption of most abundant residual carbon, most likely paraffinic wax product as suggested by the GC-MS analysis, while the second could be ascribed to highly resilient carbon species. After wax-extraction, the DSC-TGA analysis exhibited similar features to the profile before extraction, but with less pronounced weight loss of only 8 %. Tan et al. [77] reported that hexane wax-extraction under mild conditions might not remove all the wax present on the spent catalyst. Peña et al. [35,40,73] have used Soxhlet extraction to successfully remove paraffinic wax from the surface of cobalt-based FTS catalysts, however they reported that about 5% of the wax products could not be extracted by the Soxhlet

treatment. This may indicate that there is still some paraffinic wax remaining after Soxhlet wax-extraction also in our sample.

The gas stream during the TGA-DSC analysis was analysed by an on-line MS in order to determine the thermal stability of the main desorbed mass fragments. Detected fragments were associated with adsorbed carbon species. Fig. 8 shows the main MS profiles of gases from the spent catalyst before and after wax extraction TGA-DSC analysis.

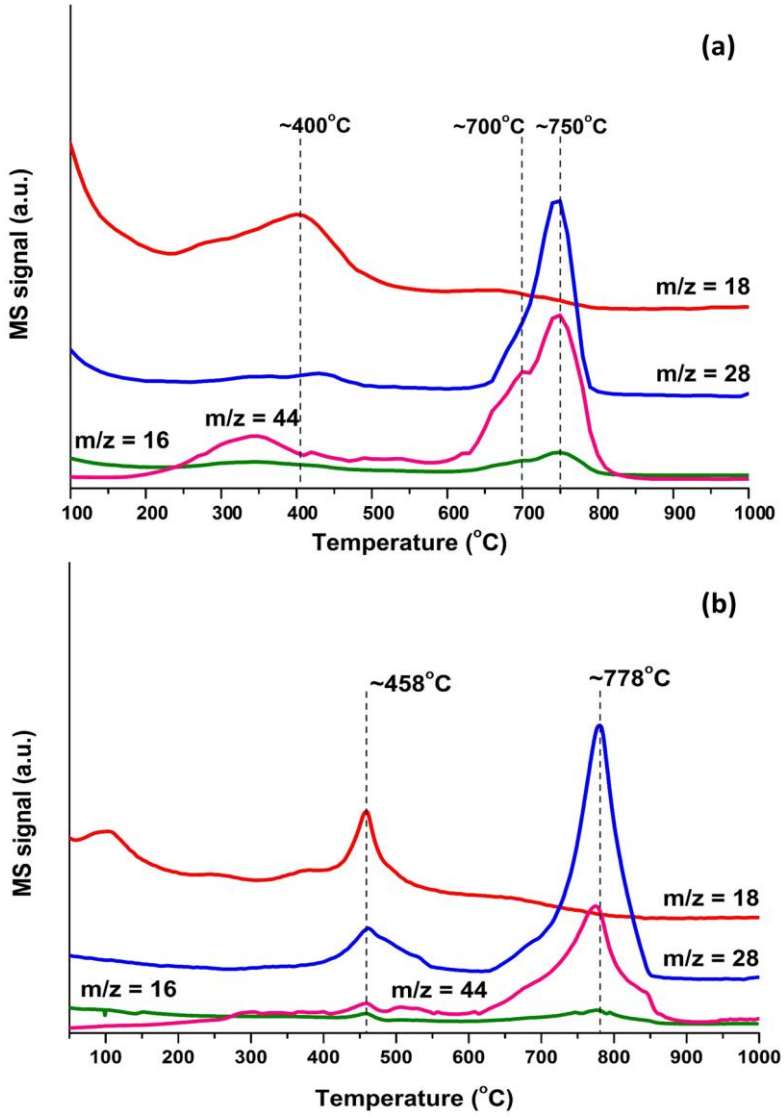

Fig. 8. MS signal during TGA analysis (a) spent catalyst (b) spent catalyst after wax-extraction.

The main mass fragments observed in Fig. 9 were m/z= 16 (CH_4, O), m/z= 18 (H_2O), m/z= 28 (CO, C_2H_2) and m/z= 44 (CO_2, C_3H_8, CH_3COH). For the spent catalyst, water desorption occurred at lower temperatures (100-150°C); the first carbon-containing gaseous species started to appear above 400°C and the second species showed a much higher signal intensity and appeared between 600-850°C. The most intense mass fragment m/z=28 can be attributed to desorption/fragmentation of any remaining hydrocarbons [35,40] while, m/z= 44 can be assigned to the main fragment for thermal decomposition of oxygenate compounds, such as alcohols or aldehydes and even carboxylate species [37]. For the spent catalyst after wax-extraction, water desorbed between 200-500°C showing a broad signal, while m/z =28 and m/z =44 mass fragments showed comparable MS intensities, suggesting that oxygenate species are still present after Soxhlet extraction. The reactivity towards hydrogen of the carbon species remaining after Soxhlet extraction was evaluated by TPH-MS experiments using a similar

methodology as previously reported [35,40]. The production of methane was detected measuring the m/z = 15 signal corresponding to the hydrogenolysis of carbon species while desorption/fragmentation of hydrocarbons (C_xH_z) was detected by monitoring the m/z=28 signal. Both signals were compared with those coming from carbide references prepared according to a previous methodology [12]. The m/z =15 and m/z =28 profiles of the wax-extracted spent catalyst and references are shown in Fig. 9.

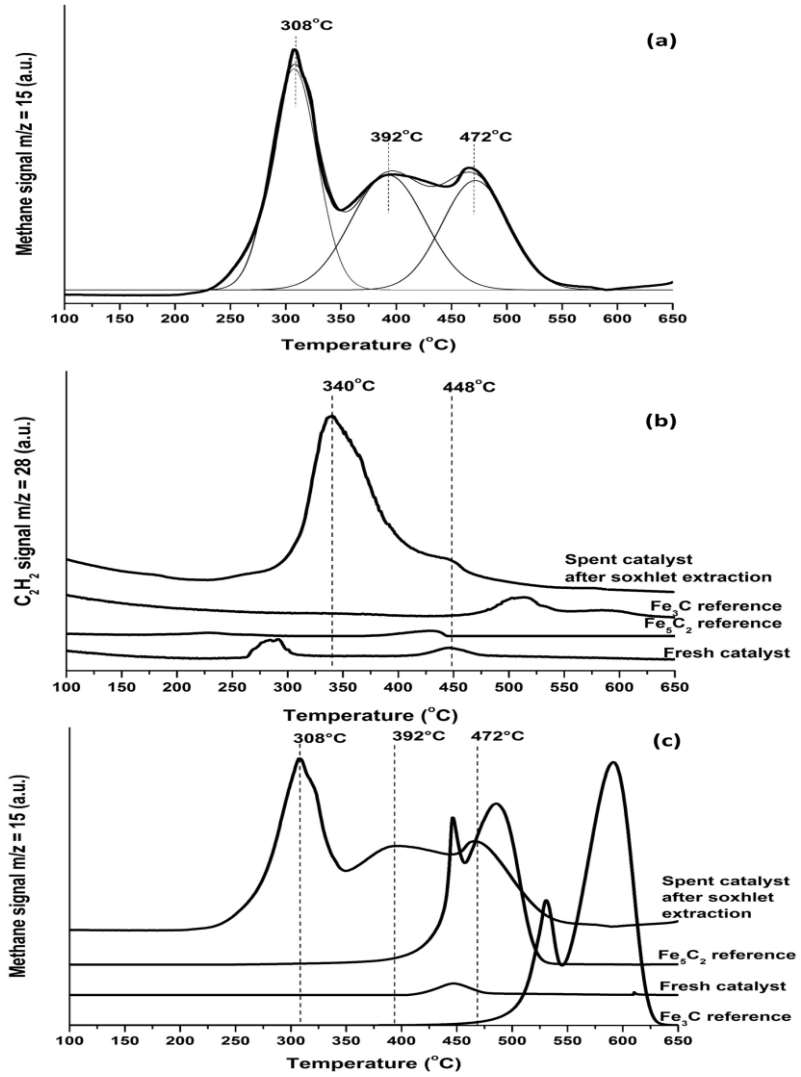

Fig. 9. Temperature-programmed hydrogen mass spectroscopy (a) m/z =15 spent catalyst wax-extracted. Spent catalyst wax-extracted compared with carbide references of Fe_5C_2 and Fe_3C (b) m/z =28 (c) m/z =15.

The methane TPH profile was deconvoluted using Gaussian fitting (Fig. 9 a) in a similar approach to what was used by Moodley et al. [34] and Peña et al. [35,40] for spent cobalt FTS catalysts. It is evident that there are three major types of carbonaceous species at ~ 300, 400 and 480°C based on their reactivity toward H_2. According to literature [78], the first species (~ 300°C) corresponds to surface carbide or atomic carbon, the second species (~ 400°C) to polymethylene or amorphous carbon aggregates, and the last species (~ 480°C) could be ascribed to ε′-$Fe_{2.2}C$ and χ-Fe_5C_2 iron carbides. However, C_2H_2 profiles suggested a main peak at ~ 340°C corresponding to the fragmentation/desorption of remaining hydrocarbons. The two carbide references were also characterised by TPH-MS and compared with CH_4 and C_2H_2 profiles of the spent catalyst. The comparison suggested that the high temperature peak detected in the CH_4 production profile of the spent wax-extracted catalyst matched with the hydrogenolysis temperature of the Hägg carbide (Fe_5C_2) reference as can be observed in Fig. 9(c), which is in good agreement with the results of Xu et al. [78]. Similarly, Pour et al. [19,21,52] studied the reactivity of surface carbon species over different iron-based FTS catalysts, reporting that the

hydrogenolysis of Hägg carbide occurs around 500°C while cementite carbide (Fe_3C) and graphite occur above 600°C and 800°C, respectively. Based on this statement and our own analysis, it is suggested that the last species detected in the CH_4 profile for the spent catalyst after wax-extraction should be associated with the hydrogenolysis of Hägg carbide, without the presence of cementite or graphite carbon. The two first CH_4 peaks can be ascribed with the hydrogenolysis of surface atomic carbon and any remaining hydrocarbons. Nevertheless, the remaining hydrocarbons are not only composed of hydrogen and carbon. Oxygen can also be present in the framework as evidenced by TGA-DSC-MS analysis (Fig. 8). These remaining hydrocarbons were extracted, separated and their molecular structure decoded using GC-MS analysis by employing the same protocol of organic extraction as previously used [35]. Fig. 10 displays the TIC chromatogram of the organic extract for the wax-extracted spent catalyst.

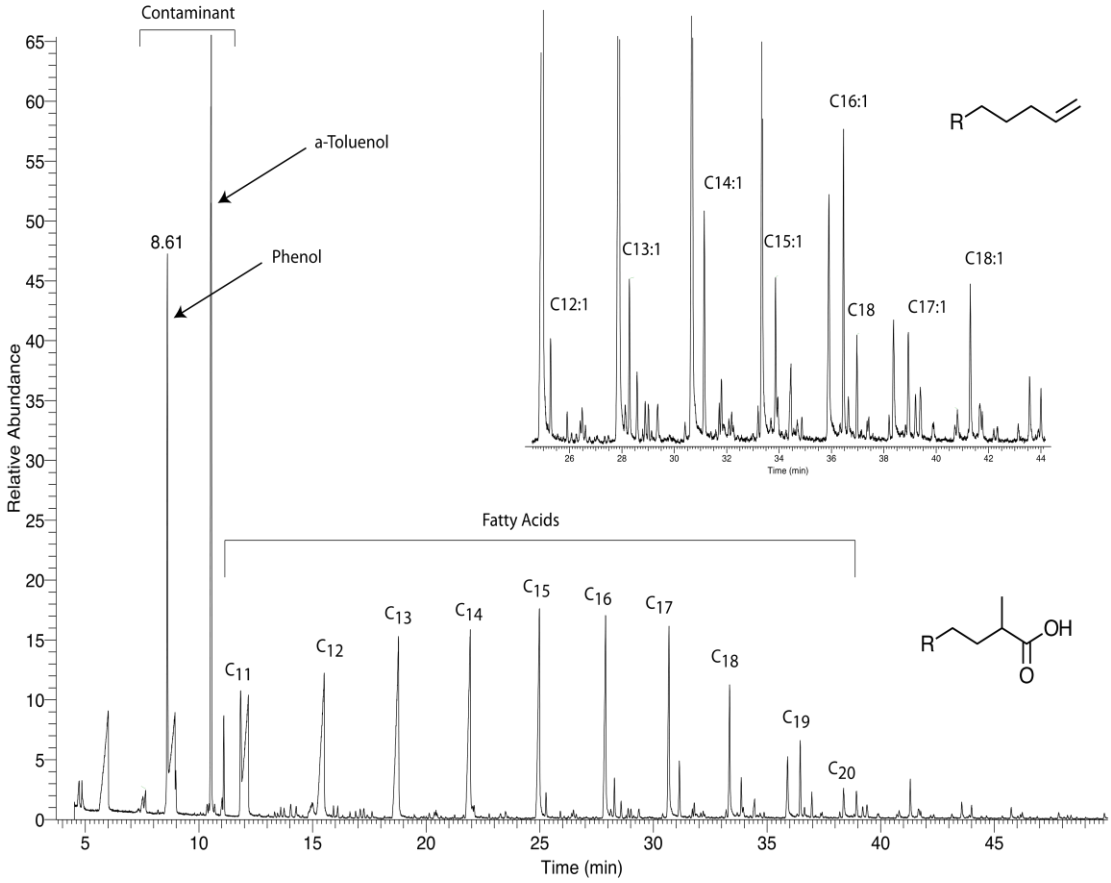

Fig. 10. TIC chromatogram of extracts from of the spent catalyst after Soxhlet wax-extraction.

Fig. 10 shows that the molecular structures of the remaining hydrocarbons were decoded. They were mainly composed of a set of branched carboxylic acids identified as 2-methyl fatty acids and other set of alpha-olefins. Primary FTS products as alpha-olefins were still present even after wax-extraction. These compounds were previously detected as strongly adsorbed carbon species after paraffinic-wax extraction for cobalt-based FTS catalysts, they were suggested as primary blocks for the formation of more complex carbon species through secondary reactions [35]. Pinard et al. [79], Peña et al. [35] and Kistamurthy et al. [37] have previously detected the presence of carboxylic acids on the surface of spent cobalt-based FTS catalysts. Peña et al. [35] and Kistamurthy et al. [37] found comparable results suggesting that the carboxylic acids have a particular preference to the alumina support. Carboxylic acids have some potentially negative effects during FTS; they can cause atomic carbon formation as a result of strongly adsorbed carboxylate species [37], they can be recombined with other reactive surface species resulting in the formation of carbonaceous residue [80] and they can generate steric hindrance once adsorbed on the catalyst surface [36]. In addition, carboxylic acids are found to be resistant towards the hydrogenation treatment over spent cobalt based-FTS catalysts [35]. Paredes-Nunes

et al. [39] reported resistant carboxylate species after H_2 treatment of spent Co-based FTS catalyst at 220°C. A possible explanation could be the formation of stable carboxylate complexes with the alumina support and/or with some metal oxide sites [36,38,39,35,37]. de Smit et al. [69] have reported the formation of carbonate species during syngas treatment over iron-based FTS catalyst at atmospheric pressure. They also reported that the carbonate species could hinder carbide formation and they slowly desorb at higher temperatures up to about 450°C [70], due probably to the formation of some stable carbonate/carboxylate complexes with iron. Fig.11 shows a schematic representation of the different oxygenate species detected on the working catalyst surface by *in situ* DRIFTS and GC-MS extraction.

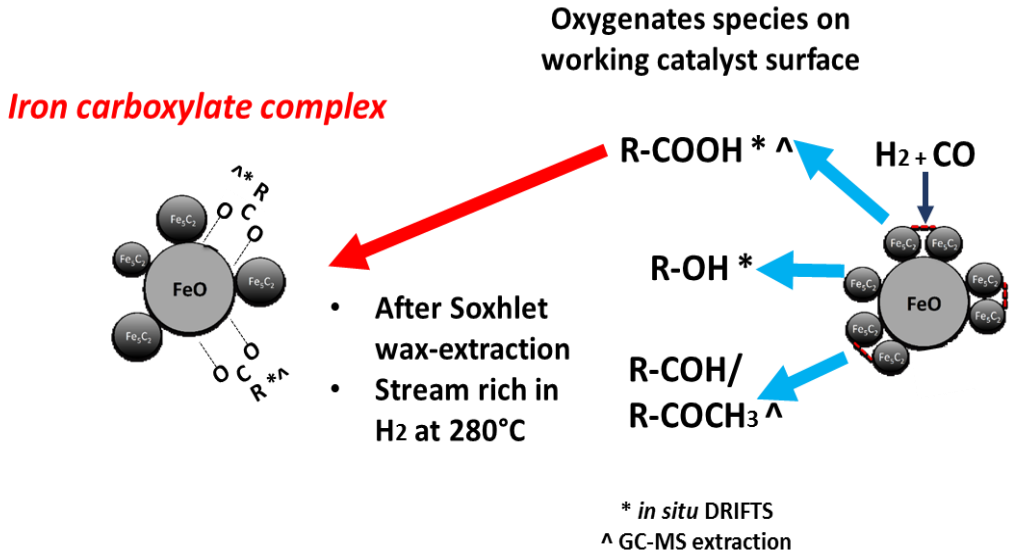

Fig. 11. Oxygenate species detected on the surface of the working catalyst.

Three oxygenate species were identified; carboxylic acids, alcohols and aldehydes/ketones. Alcohols were easily removed under a H_2–rich feed, evidenced by *in situ* DRIFTS measurements (Fig.4). 2-methyl aldehydes/2-ketones were also removed from the catalyst surface after Soxhlet wax-extraction, leaving 2-methyl fatty acids as the only strongly adsorbed oxygenate specie (Fig.10) resistant towards H_2 (Fig.4). It has been reported that iron cations Fe^{2+} and Fe^{3+} can form complexes with carboxylate ligands groups [71]. In our previous work [42], interaction of carboxylate species with the alumina support and with Fe_xO_y sites was revealed during FTS in iron-based catalysts. The formation of carboxylate complexes on Fe_xO_y sites could be a possible reason for inhibiting further iron carburization. In the present case, the detected carboxylate species are most likely forming complexes with FeO sites, because this was the only iron oxide phase present.

Transmission electron microscopy in scanning mode using energy-dispersive X-ray spectroscopy (STEM-EDX) was performed to establish the location of resilient carbon species by elemental mapping of the surface of the wax-extracted spent catalyst. To determine the location of carbon species based on their reactivity toward hydrogen, two samples were exposed to TPH analysis conditions using the same ramp (4 $Cmin^{-1}$) and stopped at 300°C and 400°C, respectively and then analysed by STEM-EDX. The first sample was initially treated in pure hydrogen at 300°C to remove the more reactive carbon species, leaving mainly the second hydrocarbon species and Hägg carbide (TPH profile Fig. 9(a)). Another sample of the wax-extracted spent catalyst was treated under pure hydrogen at 400°C, removing the first and second carbon species, leaving only carbide. A similar approach was used by Peña et al. [35] to determine location of carbon species on spent cobalt-based FTS catalysts. Fig. 12 displays the coupled TPH-MS/STEM-EDX analysis results.

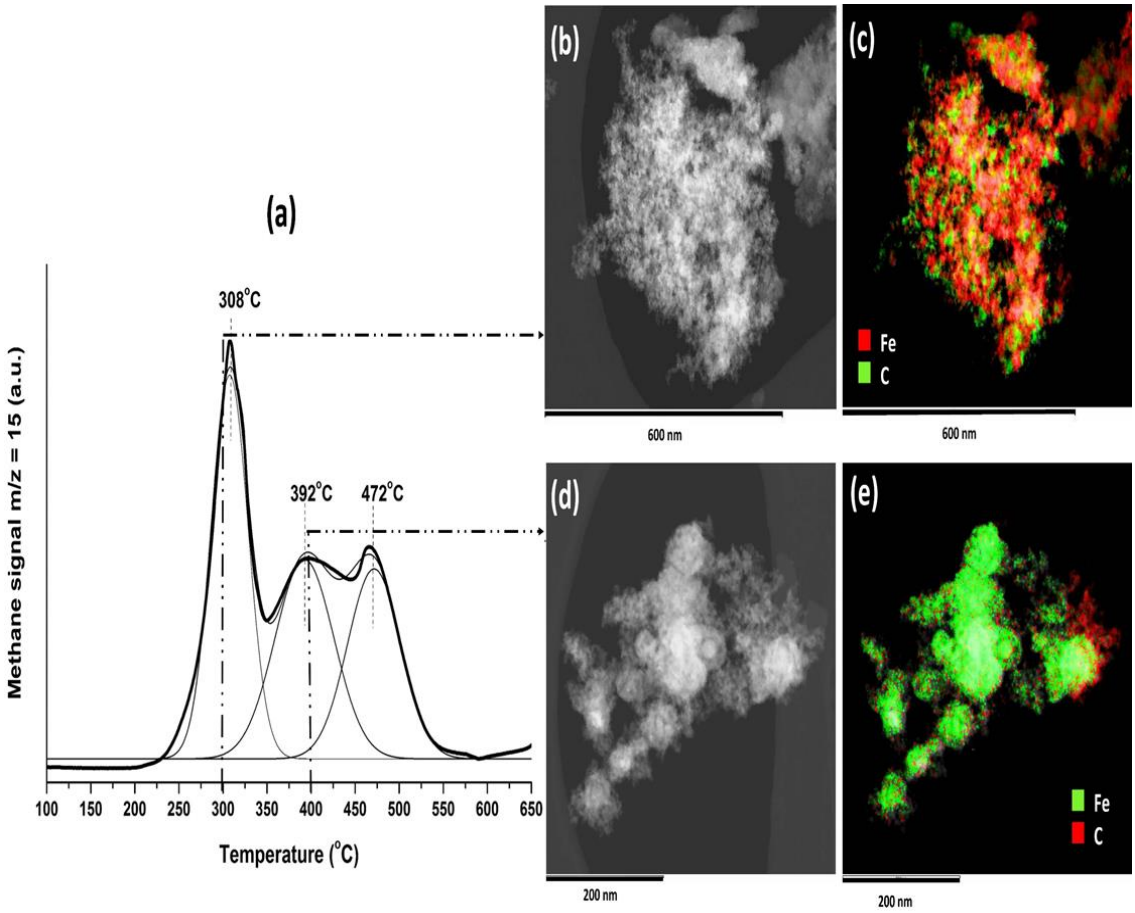

Fig. 12. TPH-MS/STEM-EDX images: (a) TPH-MS of the spent catalyst after wax-extraction, (b) high-angle annular dark-field imaging (HAADF) of spent catalyst wax-extracted after TPH at 300°C, (c) iron and carbon map, (d) HAADF of spent catalyst wax-extracted after TPH at 400°C, (e) iron and carbon map.

The sample treated at 300°C exhibited spots of carbon interacting with iron (carbon and iron maps in Fig. 12(c)) showing a heterogeneous distribution over the catalyst. Carbon deposition was especially observed on both iron phases but less on the SiO_2 (silicon map not shown). SiO_2 has lower acidity [45], and hence weaker interactions with oxygenates is expected compared to Al_2O_3, where strong interactions with carbon species especially oxygenates have been observed [35]. The treatment in hydrogen at 300°C could remove the olefinic species (Fig. 10) from the iron sites, suggesting the presence of oxygenated species such as carboxylic acids (Fig. 10) probably forming complexes with iron such as iron carboxylates. As expected, the sample treated with hydrogen at 400°C under TPH conditions showed less carbon interacting with iron (carbon and iron maps in Fig. 12(e)). However, carbon is still located on iron sites rather than on SiO_2, corresponding to Hägg carbide (Fig 9(c)). The results from the present work suggest that some carbon species once formed could interact with iron oxide sites, in this case FeO, forming stable complexes such as iron-carboxylate hampering further iron carburization [42]. Carbon deposition can occur in parallel with carbide formation during FTS [22], thus there is a competition for carbon atoms on the catalyst surface to form carbides, hydrocarbons and deleterious carbon species [12]. Deposition of inactive carbonaceous species such as carboxylates may block the access to active iron phases and also limit the degree of iron carburization [69].

Conclusions

The use of *in situ* and ex situ characterisation techniques provide strong evidence for potential deactivation mechanisms in an iron-based co-precipitated commercial catalyst. It is clear that re-oxidation/transformation of active sites, i.e. iron carbide or metallic iron is not taking place at the employed FTS operating conditions. Sintering of iron nanoparticles appears to be one of the main

causes for activity loss. Both sintering of iron oxide and iron carbide nanoparticles are observed. The sintering rate of the active phase is affected by both reaction temperature and time on stream. The sintering mechanism is believed to be a hydrothermally assisted process enhanced by the water-gas-shift reaction, which is in this case is catalysed by FeO sites and stabilised by SiO_2 due to the relatively strong FeO-SiO_2 interaction. The surface of the spent catalyst was covered by paraffinic wax, α-olefins and oxygenates such as ketones, carboxylic acids and alcohols. After paraffinic-wax extraction, the catalyst surface was mainly covered with carboxylic acids and α-olefins, suggesting that these hydrocarbons are strongly adsorbed on the catalyst surface. Three types of strongly adsorbed carbon species were identified based on their reactivity towards hydrogen: The first specie is attributed to atomic carbon, the second specie is associated to strongly adsorbed hydrocarbons (carboxylic acids and α-olefins) and the last specie corresponds to Hägg carbide. Presence of cementite or graphite could not be detected. The decomposition/desorption of strongly adsorbed carbon species on the spent catalyst after Soxhlet extraction showed high CO_2 formation probably from decomposition of oxygenate species such as carboxylate species. Carboxylic acids/carboxylate species may inhibit further catalyst carburization during FTS due to their strong interaction with iron oxide sites (FeO), forming stable complexes resistant towards hydrogenation at these conditions. The carbon species were preferentially located on the iron phases rather than on SiO_2.

Acknowledgements

This work was supported by the EU FP7-NMP-2013 project FASTCARD (Grant number 604277), and by the Research Council of Norway through the SYNKNØYT programme (Grant number 218406). Special thanks to Johnson Matthey for providing the commercial catalyst and for technical support. The STEM work was carried out at the NORTEM Gemini Centre at NTNU and supported by the NORTEM project (grant no. 197405) within the INFRASTRUCTURE program of the Research Council of Norway. The project team of the Swiss-Norwegian Beamlines (SNBL) is acknowledged for experimental assistance.

References

[1] A.Y. Khodakov, W. Chu P. Fongarland. Chem. Rev. 107 (2007) 1692-1744.
[2] J. van de Loosdrecht, F.G. Botes, I.M. Ciobîcă, A. Ferreira A, P. Gibson, D.J. Moodley, A.M Saib, J.L. Visagie, C.J. Weststrate, J.W. Niemantsverdriet. Comprehen. Inorga. Chem. II Elsevier 7. (2013) 525-557.
[3] E. de Smit, B.M. Weckhuysen. Chem. Soc. Rev. 37 (2008) 2758-2781.
[4] E. van Steen, M. Claeys. Chem. Eng. Technol. 31 (2008) 655-666.
[5] P.K. Swain, L.M. Das, S.N. Naik. Renew. Sustain. Energy Rev. 15 (2011) 4917-4933.
[6] S. Srinivas, R.K. Malik, S.M. Mahajani. Energy Sustain. Dev. 11 (2007) 66-71.
[7] A. Voronov, A. Urakawa, W. van Beek, N.E. Tsakoumis, H. Emerich, M. Rønning.. Anal. Chim. Acta 840 (2014) 20-27.
[8] N.E. Tsakoumis, R. Dehghan, R.E. Johnsen, A. Voronov, W. van Beek,J.C. Walmsley, Ø. Borg, E. Rytter, De Chen, M. Rønning, A. Holmen. Catal. Today 205 (2013) 86-93.
[9] N.E. Tsakoumis, R. Dehghan-Niri M. Rønning. J.C. Walmsley, Ø. Borg, E. Rytter, A. Holmen. Appl. Catal. A Gen. 479 (2014) 59-69.
[10] N.E. Tsakoumis, A. Voronov, M. Rønning. W. van Beek, Ø. Borg, E. Rytter, A. Holmen. J. Catal. 291 (2012) 138-148.
[11] E. de Smit, A.M. Beale, S. Nikitenko, B.M. Weckhuysen. J. Catal. 262 (2009) 244-256..
[12] E. de Smit, F. Cinquini, A.M. Beale, O.V. Safonova, W. van Beek, P. Sautet, B.M. Weckhuysen. J. Am. Chem. Soc. 132 (2010) 14928-14941.
[13] A. Espinosa, A. Serrano, A. Llavona. J. Jimenez de la Morena, M. Abuin, A. Figuerola, T. Pellegrino, J.F. Fernández,M. Garcia-Hernandez, G.R. Castro, M.A. Garcia. Meas. Sci. Technol. 23 (2012) 1-6.
[14] S. Li , R.J. O'Brien, G.D. Meitzner, H. Hamdeh, B.H. Davis, E. Iglesia. Appl. Catal. A Gen. 219 (2001) 215-222.
[15] M. Newville, Data Proces. with ifeffit , athena , & artemisa Univ. Chicago 2007.
[16] M.C. Ribeiro, G. Jacobs, B.H. Davis, D.C. Cronauer, A.J. Kropf, C.L. Marshall. J. Phys. Chem. C. 114 (2010) 7895-7903.
[17] M.C. Ribeiro, G. Jacobs, R. Pendyala, B.H. Davis, D.C. Cronauer, A.J. Kropf, C.L. Marshall. J. Phys. Chem. C. 115 (2011) 4783-4792.
[18] G.E.J. Poinern, R.K. Brundavanam, X. Thi Le, P.K. Nicholls,, M.A. Cake, D. Fawcett. Sci. Reports Nat. 4 (2014) 1-9.
[19] A. Nakhaei Pour, M.R. Housaindokht J. Zarkesh, S.F. Tayyari. J. Ind. En.g Chem. 16 (2010) 1025-

1032.
[20] A. Nakhaei Pour, S.M.K. Shahri, Y. Zamani, M. Irani, S. Tehrani..J. Nat. Gas. Chem. 17 (2008) 242-248.
[21] A.N. Pour, M.R. Housaindokht, S.F. Tayyari, J. Zarkesh J. Nat. Gas. Chem. 19 (2010) 333-340.
[22] Y. Jin, A.K. Datye. J. Catal. 196 (2000) 8-17
[23] T. Herranz, S. Rojas, F.J. Pérez-Alonso, M. Ojeda , P. Terreros, J.L.G. Fierro. Appl. Catal. A Gen. 308 (2006) 19-30.
[24] Y. Zhang, N. Sirimanothan, R.J.O. Brien, H.H. Hamdeh, H. Burtron. Stud. Surf. Sci. Catal. 139 (2001) 125-132.
[25] G. Jacobs, W. Ma, P. Gao, B. Todicb, T. Bhatelia, D.B. Bukur, B.H. Davis Catal. Today. 214 (2013) 100-139.
[26] W. Ma, Y. Ding, V.H.C. Vázquez, D.B. Bukur. Appl. Catal. A Gen. 268 (2004) 99-106.
[27] D.B. Bukur, V. Carreto-Vazquez, H.N. Pham, A.K. Datye. Appl. Catal. A Gen. 266 (2004) 41-48.
[28] H.N. Pham, A. Viergutz, R.J. Gormley, A.K. Datye. Powder Technol. 110 (2000) 96-203.
[29] S. Vasireddy, A. Campos, E. Miamee, A. Adeyiga, R. Armstrong, J.D. Allison, J.J. Spivey. Appl. Catal. A Gen. 372 (2010) 184-190.
[30] D. Wei, J.G. Goodwin, R. Oukaci, A.H. Singleton. Appl. Catal. A Gen. 210 (2001) 137-150.
[31] M. Zakeri, A. Samimi, M. Khorram, H. Atashi, A. Mirzaei. Powder Technol. 200 (2010) 164-170.
[32] R. Zhao, J.G. Goodwin, R. Oukaci. Appl. Catal. A Gen. 189 (1999) 99-116.
[33] R. Zhao, K. Sudsakorn, J.G. Goodwin, K. Jothimurugesan, S.K. Gangwal, J.J. Spivey. Catal. Today 71 (2002) 319-326.
[34] D.J. Moodley, J. van de Loosdrecht, A.M. Saib, M.J. Overett, A.K. Datye, J.W. Niemantsverdriet. Appl. Catal. A Gen. 354 (2009)102-110.
[35] D. Peña D, A. Griboval-Constant, C. Lancelot, M. Quijada, N. Visez, O. Stéphan, V. Lecocq, F. Diehl, A.Y. Khodakov. Catal. Today. 228 (2014) 65-76.
[36] D. Peña. Identification of deactivation mechanisms of cobalt Fischer-Tropsch catalysts in Slurry reactor (2013) PhD thesis University of Lille 1, France.
[37] D. Kistamurthy, A.M. Saib, D.J. Moodley. H. Prestona, I.M. Ciobîcă, W. Janse van Rensburg, J.W. Niemantsverdriet, C.J. Weststrate. Catal. Today 275 (2016) 127-134.
[38] D. Lorito, A. Paredes-Nunez, C. Mirodatos, Y. Schuurman, F.C. Meunier. Catal. Today 259 (2016) 192-196.
[39] A. Paredes-Nunez, D. Lorito, N. Guilhaume, C. Mirodatos, Y. Schuurman, F.C. Meunier. Catal. Today 242 (2014) 178-183.
[40] D. Peña, A. Griboval-Constant, V. Lecocq, F. Diehl, A.Y. Khodakov. Catal. Today 215 (2013) 43-51.
[41] N.E. Tsakoumis, A.P.E. York, D. Chen, M. Rønning. Catal. Sci. Technol. 5 (20150 4859-4883.
[42] D. Peña, L.S. Jensen, A. Cognigni, R. Myrstad, T. Neumayer, W. van Beek. ChemCatChem. (2018) 10.1002/cctc.201701673
[43] N.S. Kopelev, V. Chechersky, A. Nath. Z.L. Wang, E. Kuzmann, B.S. Zhang, G.H. Via. Chem. Mater. 7 (1995) 1419-1421.
[44] A.N. Maratkanova, R.G. Valeev. Physical-Technical Inst. Ural Branch of Russian Academy of Sciences, Russia. https://photon-science.desy.de/annual_report/files/2012/20122383.pdf.
[45] H-J. Wan, B-S. Wu, Z-C. Tao, T-Z. Lia, X. An, H-W. Xiang, Y-W. Li. J. Mol. Catal. A Chem. 260 (2006) 255-263.
[46] C.H. Zhang, Y. Yang, B.T. Teng, T.Z. Li, H.Y. Zheng, H.W. Xiang, Y. W. Li. J. Catal. 237 (2006) 405-415.
[47] V.V. Ordomsky, A. Carvalho, B. Legras, S. Paul, M. Virginie, V.L. Sushkevich, A.Y. Khodakov. Catal. Today 275 (2016) 84-93.
[48] IRON OXIDE REDUCTION EQULIBRIA. Depart. Commerce Bureau of Mines 296 (1929) United States.
[49] D. Duvenhage, N. Coville. Appl. Catal. A Gen. 298 (2006) 211-216.
[50] S.A. Eliason, C.H. Bartholomew. Appl. Catal. A Gen. 186 (1999) 229-243.
[51] M. Luo, B.H. Davis. Stud. Surf. Sci. Catal. 139 (2001) 133-140.
[52] A.N. Pour, M.R. Housaindokht, S.F. Tayyari, J. Zarkesh, M.R. Alaei. J. Mol. Catal. A Chem. 330 (2010) 112-120.
[53] A.N. Pour, M.R. Housaindokht, S.F. Tayyari, J. Zarkesh. J. Nat. Gas Chem. 19 (2010) 362-368..
[54] M.A. Richard, S.L. Soled, R.A. Fiato, B.A. DeRites. *Mater. Res. Bull*. 18 (1983) 829-833.
[55] M.D. Shroff, D.S. Kalakkad, K. E. Coulter, S.D. Köhler, M.S. Harrington, N.B. Jackson, A.G. Sault, A.K. Datye. J. Catal. 156 (1995) 185-207.
[56] A.M. Saib, D.J. Moodley, I.M. Ciobîcă, M.M. Hauman, B.H. Sigwebela, C.J. Weststrate, J.W. Niemantsverdriet, J. van de Loosdrecht. Catal. Today 154 (2010) 271-282.
[57] S. Janbroers, J.N. Louwen, H.W. Zandbergen, P.J. Kooyman. J. Catal. 268 (2009) 235-242.
[58] A.W. Burton, K. Ong, T. Rea, I.Y. Chan. Microporous Mesoporous Mater. 117 (2009) 75-90.
[59] R.A. van Santen, I.M. Ciobîcă, E. van Steen, M.M. Ghouri. Advan. Catal. 54 (2011) 127-187.
[60] H. Fang, J. Zheng, X. Luo, J. Du, A. Roldan, S. Leoni, Y. Yuan. Appl. Catal. A Gen. 529 (2017) 20-31.
[61] F.J. Pérez-Alonso, M. Ojeda, T. Herranz, S. Rojas, J.M. González-Carballo, P. Terreros, J.L.G. Fierro. Catal. Commun. 9 (2008) 1945-1948.
[62] F. Palombo, M. Paolantoni, P. Sassi, A. Morresi, R.S. Cataliotti. J. Mol. Liq. 152 (2006) 139-146.
[63] K. Arouri, P.F. Greenwood, M.R. Walter. Orga. Geo. 30 (1999) 1323-1337.

[64] F.C. Meunier, J.P. Breen, V. Zuzaniuk, M. Olsson, J.R.H. Ross. J. Catal. 187 (1999) 493-505.
[65] M. Mizuguchi, M. Nara, K. Kawano, K. Nitta. FEBS Lett. 417 (1997)153-156.
[66] W. Ning, N. Koizumi, H. Chang, T. Mochizuki, T. Itoh, M. Yamada. Appl. Catal. A Gen. 312 (2006) 35-44.
[67] S.K. Das, S. Majhi, P. Mohanty, K.K. Pant. Fuel. Process Technol. 118 (2014) 82-89.
[68] C.H. Bartholomew. Appl. Catal. A Gen. 212 (2001) 17-60.
[69] E. de Smit, M.M. van Schooneveld, F. Cinquini, H. Bluhm, P. Sautet, F.M.F. de Groot, B.M. Weckhuysen. Angew. Chem. Int. Ed. 50 (2011) 1584-1588.
[70] C. Zhang, B. Teng, Y. Yang, Z. Tao, Qinglan Hao, H. Wan, F. Yi, B. Xu, H. Xiang, Y. Li. J. Mol. Catal. A Chem. 239 (2005) 15-21.
[71] P.C.A. Bruijnincx , G. van Koten, R.J.M. Klein Gebbink. Chem. Soc. Rev. 37 (2008) 2716-2744.
[72] A.R. Barron. The Hydrogen Bond. http://cnx.org/contents/DDSt20gu@4/The-Hydrogen-Bond.
[73] D. Peña, A. Griboval-constant, F. Diehl, V. Lecocq, A.Y. Khodakov. ChemCatChem 5 (2013) 728-731.
[74] J.C. Park, S.C. Yeo, D.H. Chun, J. T. Lim, J-I. Yang, H-T. Lee, S. Hong, H.M. Lee, C.S. Kim, H. Jung. J. Mater. Chem. A. 2 (2014) 14371-14379.
[75] A.S. Luyt, I. Krupa. Thermochim. Acta 467 (2007) 117-120.
[76] G.R. Moradi, M.M. Basir, A. Taeb, A. Kiennemann. Catal Commun. 4 (2003) 27-32.
[77] K. Fei Tan, J. Xu, J. Chang, A. Borgna, M. Saeys. J. Catal. 274 (2010) 121-129.
[78] J. Xu, C.H. Bartholomew. J. Phys. Chem. B. 109 (2005) 2392-2403.
[79] L. Pinard, Bichon P, Popov, J.L. Lemberton, C. Canaff, F. Maugé, P. Bazin, E. Falabella S.-Aguiar, P. Magnoux. Appl. Catal. A Gen. 406 (2011) 73-80
[80] T. Yoshikawa, T. Yagi, S. Shinohara, T. Fukunaga, Y. Nakasaka, T. Tago, T. Masuda. Fuel Process Technol. 108 (2013) 69-75.